Science Advances
AAAS

advances.sciencemag.org/cgi/content/full/6/7/eaay8189/DC1

Supplementary Materials for

On the glacial-interglacial variability of the Asian monsoon in speleothem $\delta^{18}O$ records

G. Liu*, X. Li, H.-W. Chiang, H. Cheng, S. Yuan, S. Chawchai, S. He, Y. Lu, L. T. Aung, P. M. Maung, W. N. Tun, K. M. Oo, X. Wang*

*Corresponding author. Email: gxliu@ntu.edu.sg (G.L.); xianfeng.wang@ntu.edu.sg (X.W.)

Published 12 February 2020, *Sci. Adv.* **6**, eaay8189 (2020)
DOI: 10.1126/sciadv.aay8189

The PDF file includes:

Supplementary Text
Fig. S1. Locations of the study sites.
Fig. S2. Climatology of relevant cities.
Fig. S3. Images of stalagmite samples.
Fig. S4. Age models.
Fig. S5. Replication test on stable isotope data from PDM02.
Fig. S6. Scatter plot of $\delta^{18}O$ versus $\delta^{13}C$.
Fig. S7. The three obtained speleothem $\delta^{18}O$ records.
Fig. S8. Comparison of the CBoB and Mawmluh cave records.
Fig. S9. Comparison of orbital AM records and Vostok atmospheric molecular oxygen $\delta^{18}O$ record.
Fig. S10. Spatial-temporal comparison of speleothem $\delta^{18}O$ records from the coastal Indian Ocean and southern China.
Fig. S11. Ice volume and temperature effects.
Fig. S12. Spatial-temporal comparison of speleothem $\delta^{18}O$ records from mainland Southeast Asia over the past 40 ka.
Fig. S13. Calculation of rainfall $\delta^{18}O$ gradient across mainland Southeast Asia.
Table S1. A list of the studied speleothem samples and their cave locations.
Table S2. Rainfall oxygen isotopic compositions across mainland Southeast Asia.
Table S3. Calculations of water vapor loss over the CBoB site.
Legends for data S1 and S2
References (*63–91*)

Other Supplementary Material for this manuscript includes the following:

(available at advances.sciencemag.org/cgi/content/full/6/7/eaay8189/DC1)

Data S1 (Microsoft Excel format). ^{230}Th dating results, with errors within 2σ (95% in confidence).
Data S2 (Microsoft Excel format). Stable isotope compositions.

Supplementary Text

Isotope equilibrium tests

To confirm that carbonate (calcite or aragonite) is deposited under isotopic equilibrium conditions before attempting any climatic interpretation of stalagmite $\delta^{18}O$, we first calculated the correlation factors between $\delta^{18}O$ and $\delta^{13}C$ for each sample (Fig. S6). Their low R^2 values argue against kinetically driven isotope fractionation during speleothem growth *(63)*.

We then compared rainfall $\delta^{18}O$ inferred from near-modern speleothem $\delta^{18}O$ with amount-weighted annual rainfall $\delta^{18}O$ measured at nearby cities (Fig. S2, and Table S2). Note two major cities, Yangon and Bangkok, are located near our CBoB caves (Fig. S1). The isotope analysis of Yangon samples was based on only 3-years' dataset of monthly precipitation samples collected more than 50 year ago (Data from: https://nucleus.iaea.org/wiser/index.aspx). We therefore decided to use the climatological data from Bangkok instead, which comprises observational data over 40 years. The amount-weighted annual $\delta^{18}O$ of Bangkok rainfall is -6.7±1.0‰ relative to Vienna Standard Mean Ocean Water (VSMOW). Although the rainfall $\delta^{18}O$ signal in Bangkok may be contaminated by a minor moisture contribution from the South China Sea, the signal has been demonstrated to be very similar to the rainfall $\delta^{18}O$ from Chiangmai and Sukhothai in northern Thailand *(64)*, located even closer to the CBoB site. Also note that, to date, no rainfall isotope values have been measured for the CM site, neither for the broad Shan Plateau. We therefore calculated local modern rainfall $\delta^{18}O$ (~-7.6‰ VSMOW) from IsoMap (http://wateriso.utah.edu/waterisotopes/pages/data_access/oipc.html) *(65)*. Nevertheless, the agreement between amount-weighted annual rainfall $\delta^{18}O$ and modern speleothem $\delta^{18}O$ at the three sites further suggests that speleothem carbonates were deposited under isotopic

equilibrium conditions, with particularly the near-modern speleothem $\delta^{18}O$ values being robust (Table S2).

A more robust equilibrium test involves replication of isotopic records among samples and across caves *(2, 60, 66, 67)*. Our speleothem records from Yunnan and Myanmar can be broadly correlated on millennial to orbital timescales with records from caves several thousand kilometers away in the Asian Monsoon region over their contemporaneous growth periods (Figs. S8-S10) *(1, 2, 20, 60, 61)*. Similar correlations also exist between the records from the CBoB, Mawmluh *(21, 26)*, and Bittoo caves *(22)* in northern India.

We discarded the top 8 mm of sample A14 as it is unclear whether the calcite is of original deposition or transformed from aragonite through diagenesis. For its aragonite portion, we applied a 0.8‰ aragonite-calcite correction *(68, 69)*. The corrected stalagmite $\delta^{18}O$ values are in very good agreement during the overlapping periods with the data from calcite sample A15.

With the above lines of evidence, we can reasonably conclude that the speleothem samples collected in our study most likely grew under isotopic equilibrium conditions. The variation of carbonate $\delta^{18}O$ was therefore largely controlled by local precipitation $\delta^{18}O$ and cave temperature at the time of carbonate precipitation.

Calculations based on the idealized Rayleigh distillation model

Our calculations employing idealized Rayleigh distillation model reveal, firstly, that ~3.7‰ shift in the CBoB speleothem $\delta^{18}O$ corresponds to 56% reduction of ISM rainfall during the LGM, and secondly, that temperature alone can explain ~1.7‰ out of the total ~3‰ difference in the $\delta^{18}O$ gradient between the LGM and the present across mainland Southeast Asia. The robustness of our calculations depends on the validity of several assumptions.

The requisite assumption of the idealized Rayleigh distillation model is isotope equilibrium when water evaporates and condenses. While in nature condensation is approximately an

equilibrium process, evaporation is mostly kinetic. It is known that water vapor over the oceans has more negative $\delta^{18}O$ values than predicted by the equilibrium conditions due to kinetic fractionation. Accounting for kinetic effect in our calculations would then have resulted in slightly larger values of vapor remaining in air mass (*f*) at the CBoB site for both today and the LGM. However, it is challenging to quantify how much *f* could have changed in the LGM, and how such change could compromise our estimated rainfall amount reduction, because very little knowledge is available on the RH and wind speed over tropical oceans during the LGM *(70)*.

We evaluated the contribution of kinetic fractionation using the following approach. We have shown that the 3.7‰ LGM-Modern difference in speleothem $\delta^{18}O$ of CBoB can be translated to ~2‰ changes in precipitation $\delta^{18}O$ after correcting for both cave temperature and ice volume effects; the ~2‰ changes are largely consistent with isotope records from groundwater *(30)* and the BoB sea surface water *(5)*, and mostly resulted from reduction in rainfall (amount effect). This 2‰, or even a larger change, cannot be accounted for if the oxygen isotope kinetic fractionation factor between ocean water and vapor was significantly smaller during the LGM than today.

The kinetic process is controlled by oceanic surface RH and wind speed, with generally lower RH and high wind speeds leading to stronger kinetic fractionation, although the influence of wind speed could be complex *(71-74)*. During the glacial periods, the sea surface RH was likely similar *(75)* or slightly higher *(72)* compared to the present, while the wind speed was larger *(72)*, making it difficult to precisely evaluate the changes in the kinetic fractionation factor. We estimate conservatively the differences in the kinetic fractionation factor under a hypothetical LGM scenario when the oceanic surface RH increased to 90% from today's 80%, while the wind speed did not change, using the equation *(76)*

$$\Delta\varepsilon^{18}O = 14.2 \times (1 - RH) \quad \text{(Eq.9)}$$

where $\Delta\varepsilon^{18}O$ is the kinetic enrichment factor. Therefore, $\Delta\varepsilon^{18}O$ changed from today's 2.8‰ to LGM's 1.4‰. Under this scenario, the 1.4‰ (that is, 2.8‰ - 1.4‰) out of the observed 2‰ changes in rainfall oxygen isotope can be attributed to the change in kinetic fractionation. The remaining 0.6‰ still indicates a reduction of ISM rainfall.

The influence of kinetic fractionation on the continent is even harder to quantify. Yet, it can be critical, as temperature alone explains only ~1.7‰ out of the total ~3‰ difference in the $\delta^{18}O$ gradient between the LGM and the present across mainland Southeast Asia. Thus, moisture recycling must have changed from being dominantly driven by transpiration to being mostly driven by evaporation (Fig. S13).

Another requisite parameter in the idealized Rayleigh model is temperature. The uncertainty in the LGM temperature estimation at the CBoB cave sites is probably within 1 °C. We realize that water vapor loss is not sensitive to such small temperature changes (Table S3), consistent with previous observations *(32)*. The continental $\delta^{18}O$ gradient change, however, is sensitive to temperature gradient changes (Fig. S13), because the vapor amount remaining in the air column (i.e., PWV) is temperature dependent. Considering temperature changes reconstructed by both climate records and model simulations *(5, 20, 23, 24, 27, 29, 34, 57)*, we selected a modest increase of ~2 °C/1,000 km in the regional temperature gradient during the LGM (see Materials and Methods).

The PWV is the integrated water vapor density (or absolute humidity, AH) in a vertical air column. Its precise measurement requires knowledge of many climate parameters in the air column, and remains challenging even with the help of cutting-edge technologies *(77-79)*. We made first-order estimates of annual mean PWVs using limited available surface-level parameters (i.e., temperature and RH). Under the assumption that water vapor density

decreases exponentially with height by a factor of 0.439 km^{-1} *(36)*, PWV can be calculated using surface-level AH from the equation

$$PWV = AH/0.439 \quad \text{(Eq. 10)}$$

The AH (in g m^{-3}) can be calculated from the equation

$$AH = (C \times e \times RH)/T \quad \text{(Eq. 11)}$$

where T is the temperature (in kelvin); C is a constant with a value of 2,165 g K kJ^{-1}; *e* is the saturation vapor pressure (in kPa); and RH is relative humidity. Combining Eq. 10 and Eq. 11, we can get Eq. 5. The major uncertainty in Eq. 10 is that the decreasing factor (0.439) is less accurate during winter. But its contribution to the amount of vapor is small, and therefore the absolute error of PWV remains small *(36)*. To further verify our calculations, we re-calculated the PWVs using another equation *(80, 81)*

$$\ln(PWV) = 0.1102 + 0.06138 \times T_{dp} \quad \text{(Eq. 12)}$$

where T_{dp} is the surface dew-point temperature (in Celsius), which can be approximated using the equation *(82)*

$$T_{dp} \approx T_c - (100 - RH) / 5 \quad \text{(Eq. 13)}$$

where T_c is the surface temperature (in Celsius), and RH (in percentage) is relative humidity.

Given a relative humidity of 100%, although the PWVs calculated using the two methods show slight discrepancies, we reach almost identical results by replacing Eq.5 with Eq. 12. For example, the calculated 56% reduction in ISM rainfall changes to 55%, and the calculated ~1.7‰ (from 6.0‰ to 7.7‰) change in the $\delta^{18}O$ gradient becomes ~1.5‰ (from 6.4‰ to 7.9‰). Nevertheless, both equations suggest that PWV increases with temperature at a rate of ~6%/°C, consistent with the Clausius-Clapeyron relation *(78, 83)*.

Note that RH on the continent is in fact not 100% (for example, ~75% in Yangon, Bangkok, and Kunming, today), and could be slightly higher *(72)* or remain the same *(75)* during the LGM. We applied ~75% RH for today and 90% RH during the LGM, and found that the rain amount lost with respect to modern value changed from 56% to 67% (Table S3). Nevertheless, regardless of the changes in RH, the rain amount in the region must have been substantially lower than at the present day, if the isotope change is largely controlled by Rayleigh type fractionations. The isotope gradient calculation is not influenced as along as the surface RH remains largely constant spatially, which seems to be the case today *(84)*, as surface RH at different locations will be cancelled out when calculating *f*. While we cannot quantify the spatial pattern of surface RH during the LGM, but assuming that surface RH in the catchment did not change spatially during the LGM *(75)*, our calculation can capture a broad picture of isotope depletion at a higher rate under lower temperatures and a larger temperature gradient.

In summary, although several assumptions are required, our calculations based on idealized Rayleigh fractionation does point out that ISM rainfall was reduced significantly during the LGM, and that temperature is an important, but not the only, controlling factor in observed changes in the continental isotope gradient.

Supplementary Figures

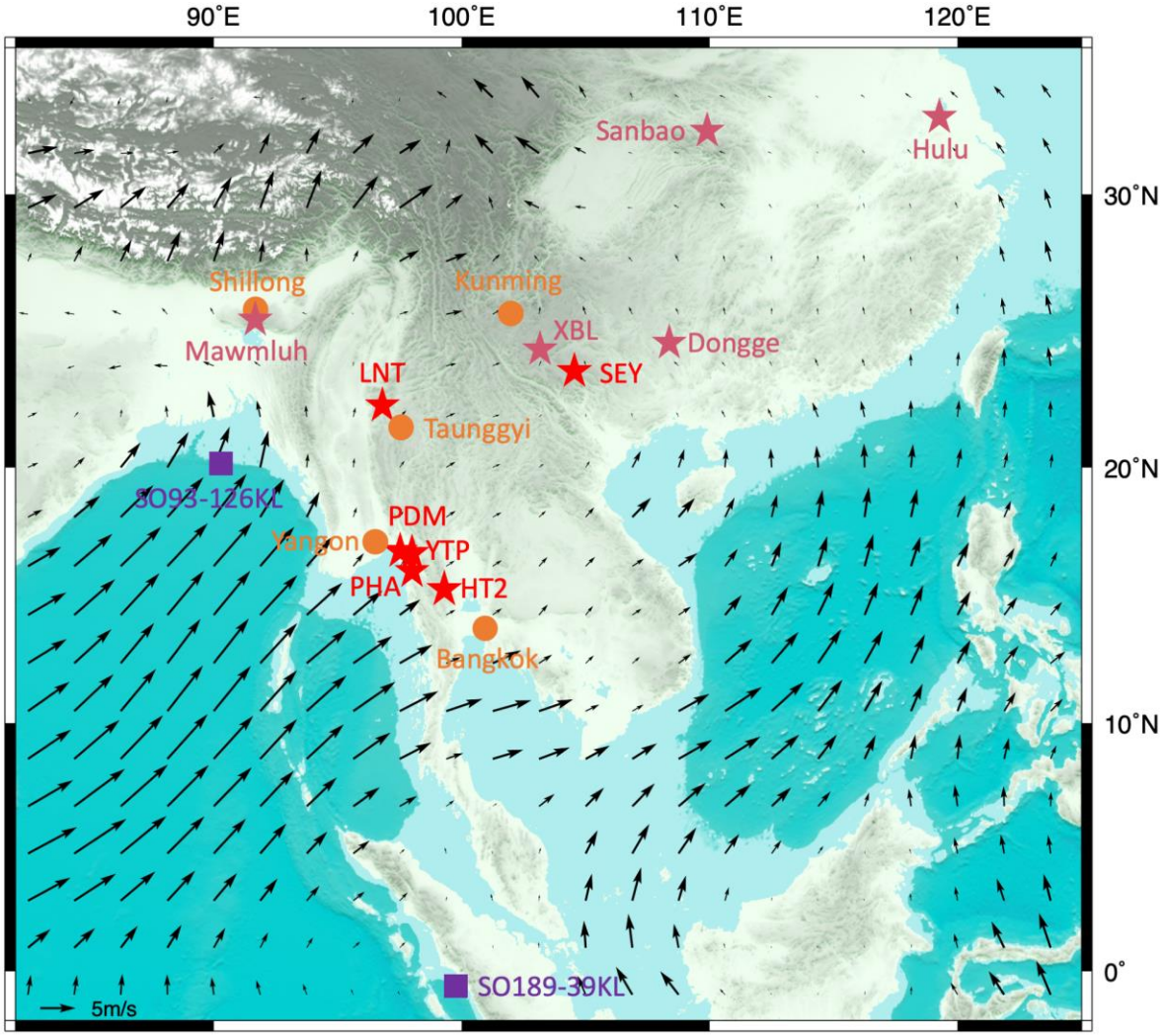

Fig. S1. Locations of the study sites. Cave sites (red stars: sites for this study; pink stars: published cave sites in the region *(1, 2, 20, 21, 26, 60-62, 85)*), marine sediment cores SO93-126KL (square) *(27)* and SO189-39KL *(39)*, and major cities (circles) referred to in this study.

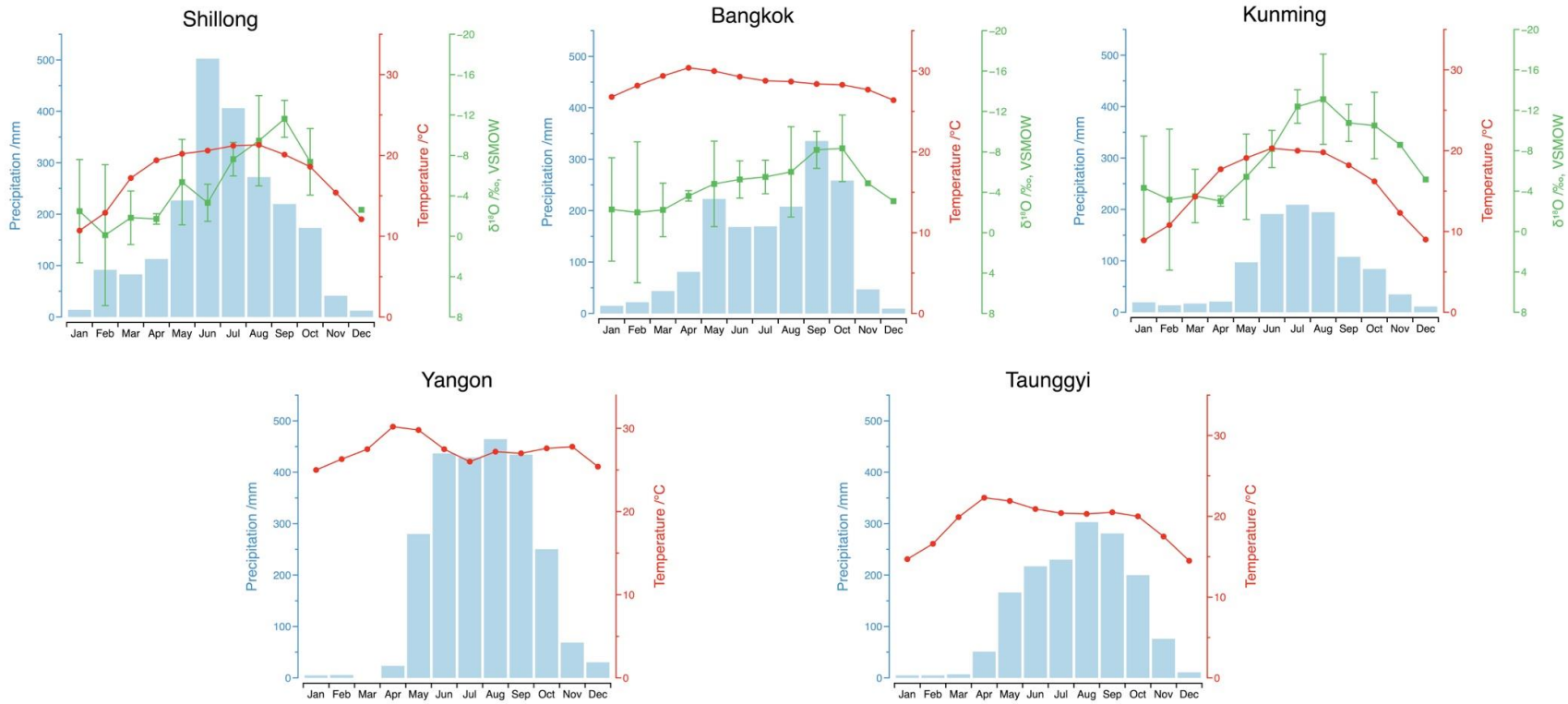

Fig. S2. Climatology of relevant cities. Data are from the IAEA (https://nucleus.iaea.org/wiser/index.aspx) and the United Nation Statistical Database (http://data.un.org/Explorer.aspx?d=CLINO). (Note that the temperature and rainfall data from the two databases have minor discrepancies.)


HT2-1
HT2-2
PDM02
PHA02
YTP01
LNT01
LNT04
LNT05
LNT09u
LNT09
LNT02
LNT09b
A14
A15
BF2
SY10
JJ03
JJ06
SL08
SL10
XR05

Fig. S3. Images of stalagmite samples. CBoB samples: HT2-1 and HT2-2 are from Hin Thun No.2 cave; PDM02 is from Padamya cave; PHA02 is from Phabaung Gu cave; and YTP01 is from Ya Thea Phyan Gu cave. CM samples: LNT01, LNT02, LNT04, LNT05, and LNT09 are from Lin Noe Twin cave. SEY samples: A14 and A15 are from an unnamed cave in SEY; BF2 is from Baifen cave; SY10 is from Shuiyuan cave; JJ03 and JJ06 are from Jiangjun cave; SL08 and SL10 are from Shuanglong cave; and XR05 is from Xianren cave.

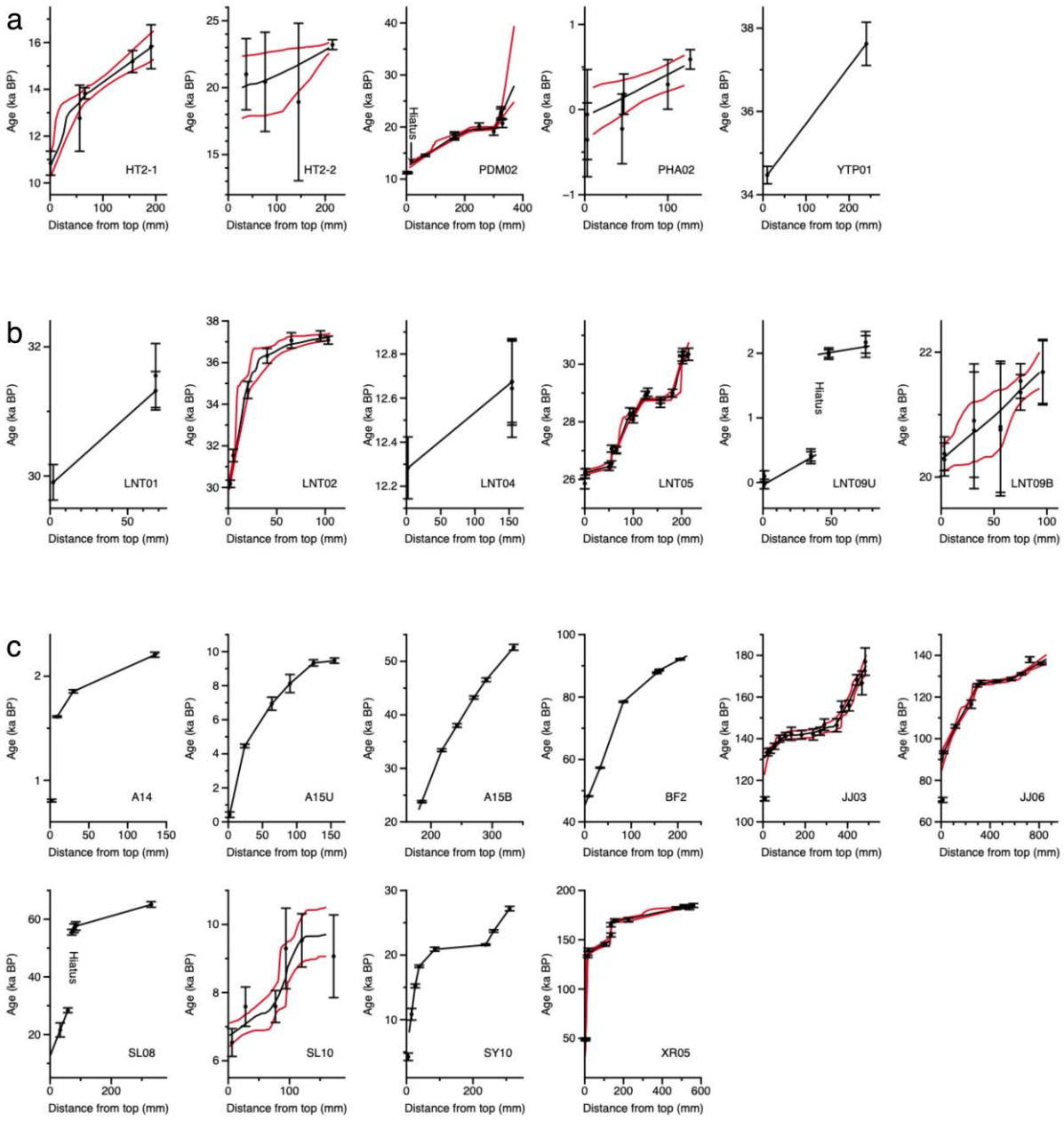

Fig. S4. Age models. All ages are reported in thousands of years before present or ka BP (BP refers to 1950 AD). The age errors indicated in the plots are 2σ-errors. **a).** Plots of age versus depth for stalagmites from the CBoB caves. StalAge method *(54)* was used to establish the chronology for HT2-1, HT2-2, PDM02, and PHA02. The red lines indicate 95% confidence intervals calculated by a Monte Carlo simulation fitting. The top ~1cm above the hiatus in sample PDM02 was assumed to grow steadily between 11.2 ka and 11.5 ka. Linear interpolation was used to establish the chronology for YTP01. **b).** Plots of age versus depth

for stalagmites from CM LNT cave. StalAge method *(54)* was used to establish the chronology for LNT02, LNT05, and LNT09B. The red lines indicate 95% confidence intervals calculated by a Monte Carlo simulation fitting. Linear interpolation was used to establish the chronology for the rest of the samples. **c).** Plots of age versus depth for stalagmites from SEY caves. StalAge method *(54)* was used to establish the chronology for JJ03, JJ06, SL10, and XR05. The red lines indicate 95% confidence intervals calculated by a Monte Carlo simulation fitting. Linear interpolation was used to establish the chronology for the rest of the samples.

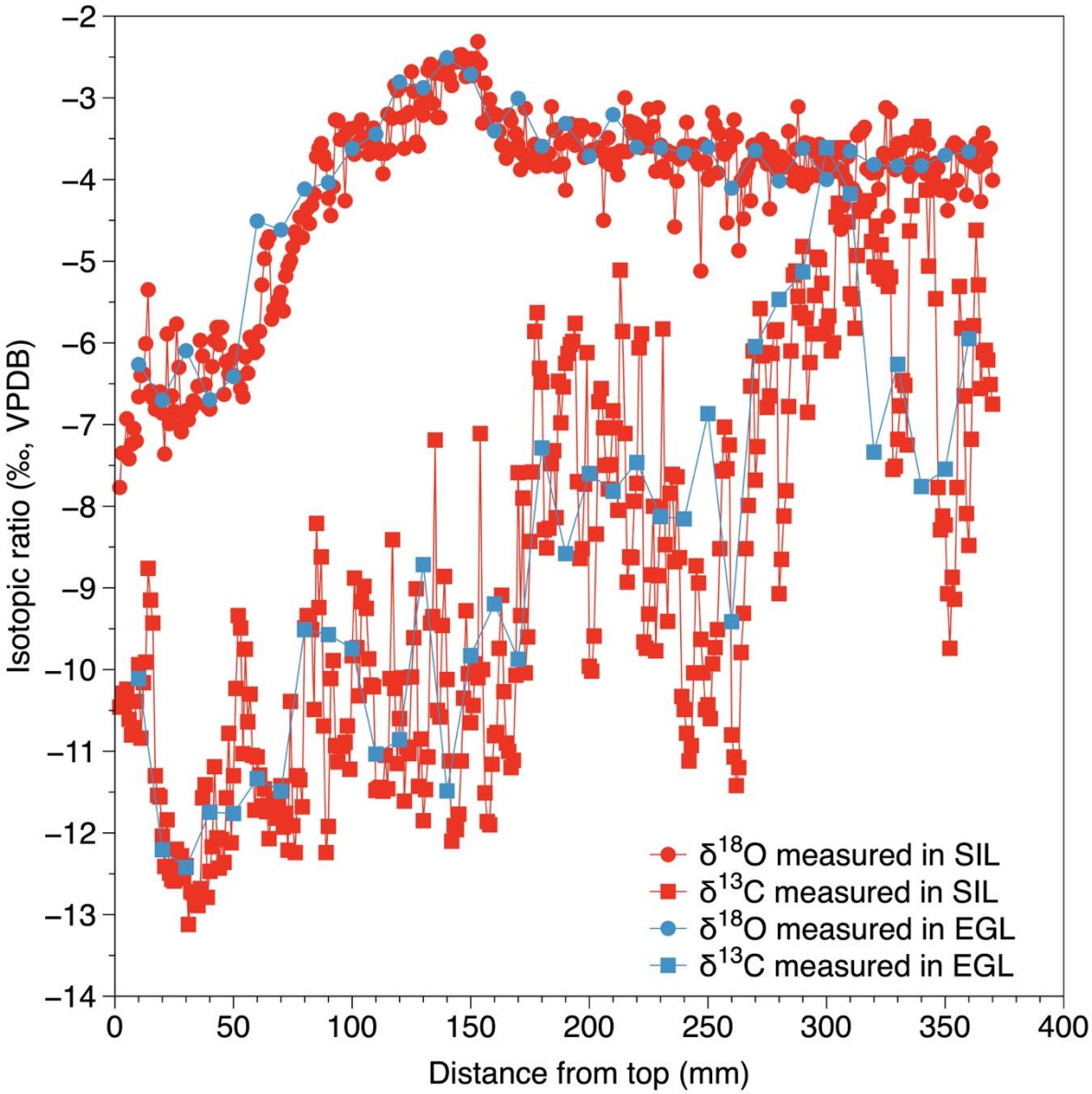

Fig. S5. Replication test on stable isotope data from PDM02. The two datasets were obtained from different transects along the growth axes, and the measurements were done at two different laboratories, the EGL of the EOS/ASE at Nanyang Technological University in Singapore and the SIL at Nanjing Normal University in China, respectively.

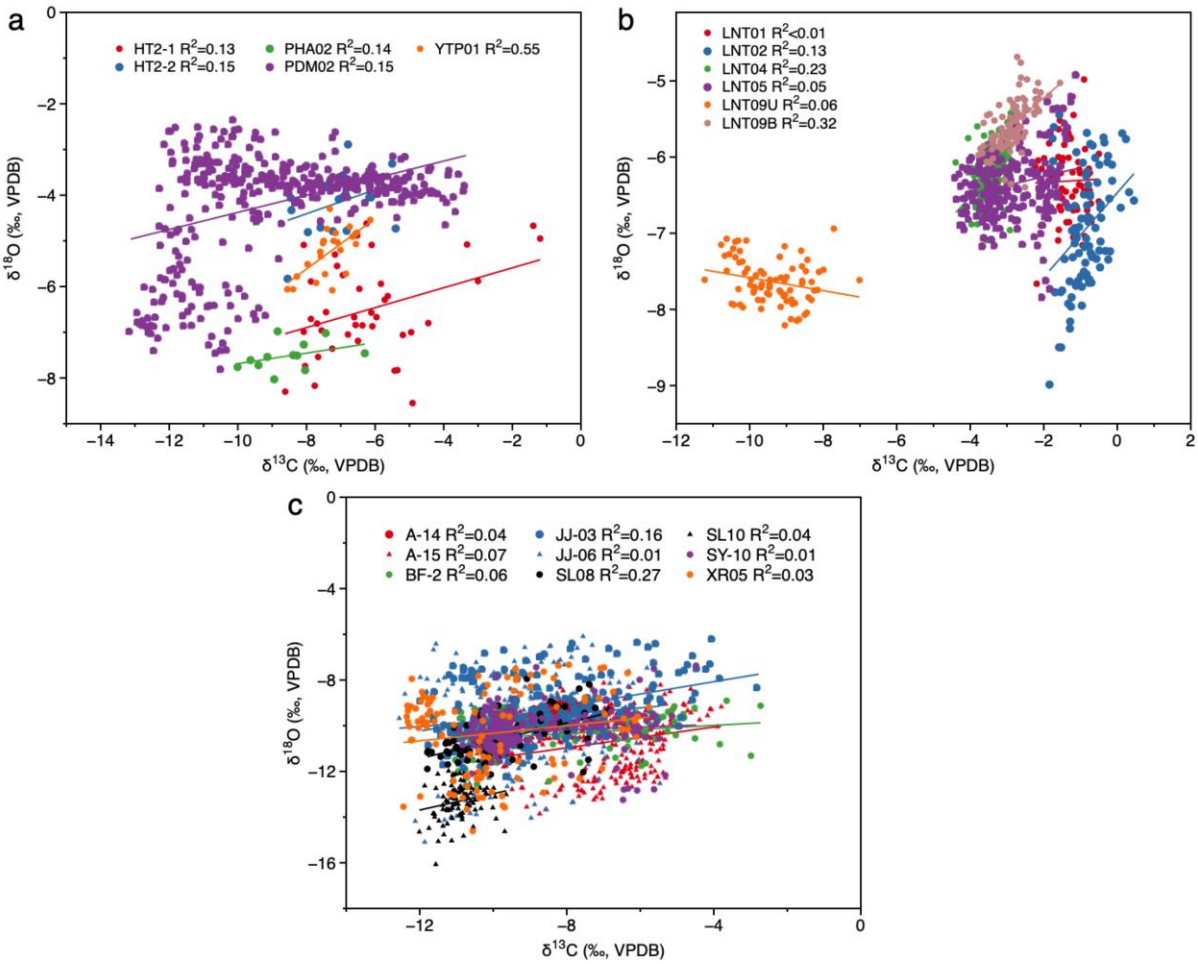

Fig. S6. Scatter plot of $\delta^{18}O$ versus $\delta^{13}C$. a). for the CBoB stalagmites; **b).** for the CM stalagmites; and **c).** for the SEY stalagmites. The low correlations between $\delta^{18}O$ and $\delta^{13}C$, as indicated by R^2 values, suggest that the speleothem carbonates were likely deposited under isotopic equilibrium conditions, with negligible influence of kinetic fractionation.

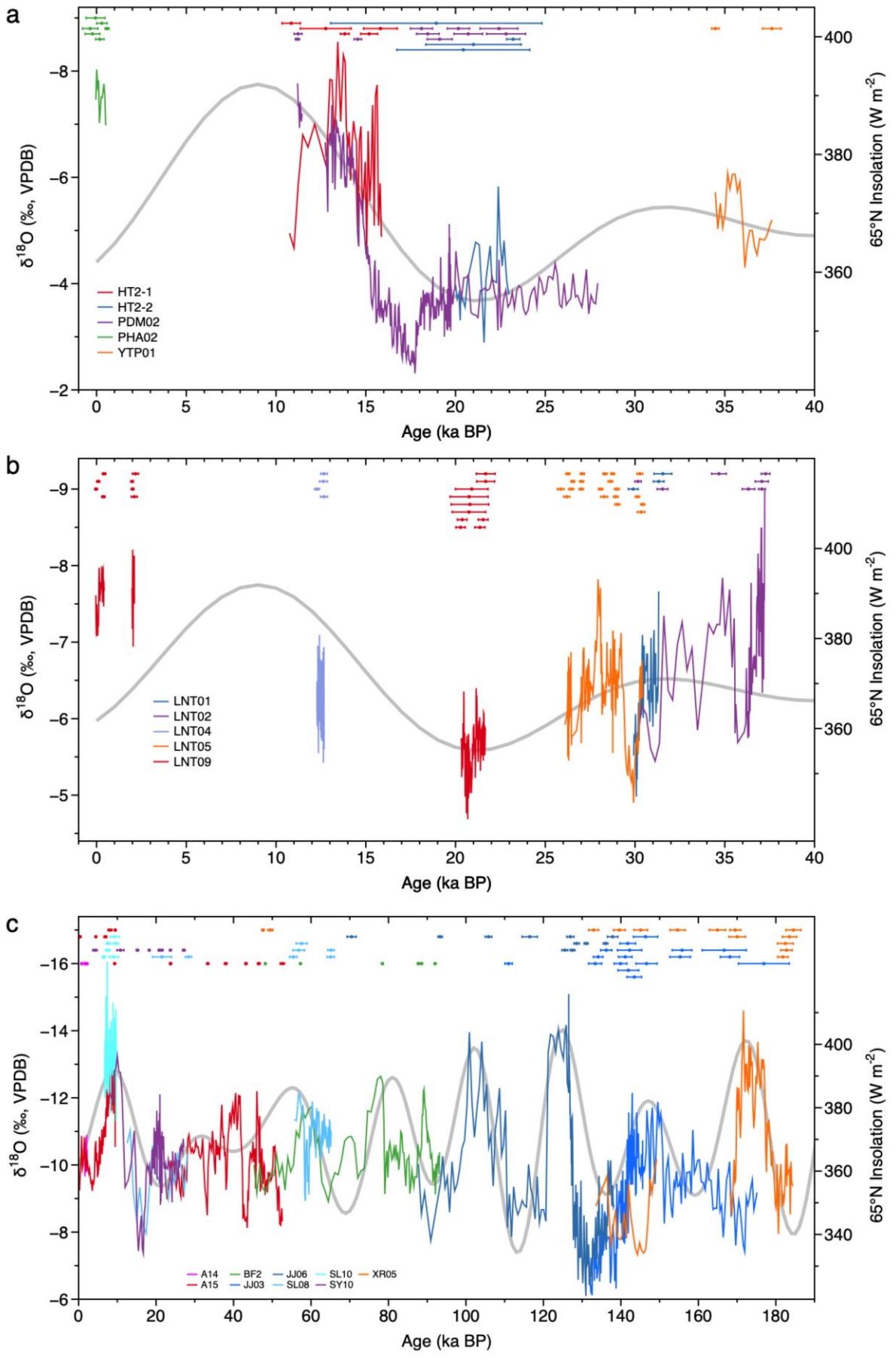
a
δ18O (‰, VPDB)
65°N Insolation (W m-2)
Age (ka BP)
HT2-1
HT2-2
PDM02
PHA02
YTP01
b
δ18O (‰, VPDB)
65°N Insolation (W m-2)
Age (ka BP)
LNT01
LNT02
LNT04
LNT05
LNT09
c
δ18O (‰, VPDB)
65°N Insolation (W m-2)
Age (ka BP)
A14
A15
BF2
JJ03
JJ06
SL08
SL10
SY10
XR05

Fig. S7. The three obtained speleothem $\delta^{18}O$ records. The $\delta^{18}O$ profiles and dating error bars (2σ) are color coded. 65°N summer (JJA) insolation (grey) is also included for comparison. **a).** The CBoB records. The apparent offset of HT2-1 and PDM02 around 11ka is largely due to the low sampling resolution and relatively large uncertainties in chronology. **b).** The CM record. **c).** The SEY records. The apparent offsets between the samples around 60 ka, 90 ka, and 138 ka are largely due to the low sampling resolution and relatively large uncertainties in chronology.

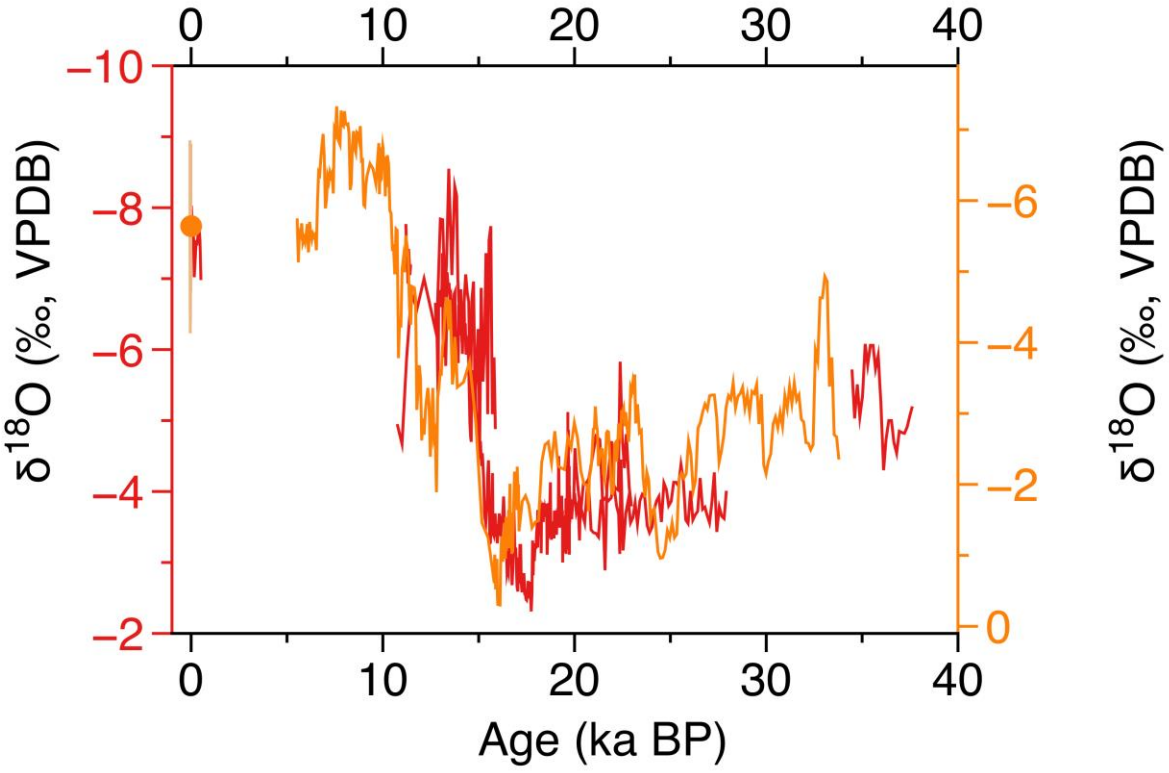

Fig. S8. Comparison of the CBoB and Mawmluh cave records. The CBoB $\delta^{18}O$ record (red) largely replicates the compiled Mawmluh record (orange) within dating errors in their contemporaneous growth intervals, which suggests that both records are robust and the climate signal is coherent across the region. The Mawmluh record consists of $\delta^{18}O$ data from calcite stalagmite MWS-1 (late glacial to early Holocene) *(21)* and aragonite stalagmite MAW0201 (last ~50 years) *(26)*, in which the latter was shifted 0.8‰ negatively to account

for different water-rock isotope fractionation between aragonite and calcite *(68, 69)*. Since the modern MAW0201 record has a very high sampling resolution (~8 points per year), it shows large seasonal variability. We calculated its mean $\delta^{18}O$ value (orange dot), and such a value (-7.7 ± 0.5‰ after aragonite-calcite correction) is >3‰ lower than the LGM values of MWS-1 (-4.6 ± 0.4‰). The Mawmluh record consistently exhibits $\delta^{18}O$ values ~2.1‰ higher than the CBoB record. As the modern rainfall $\delta^{18}O$ values are essentially the same at the two locations (-6.7 ± 1.0‰ in Bangkok, a major city near the CBoB caves, and -6.1 ± 2.2‰ in Shillong, the closest major city to Mawmluh Cave. Data from: https://nucleus.iaea.org/wiser/index.aspx), the offset in the two records can largely be explained by the difference in surface temperatures due to the different altitudes of the cave sites. The CBoB caves are located at present-day sea level, while Mawmluh cave is ~1,100 m above sea level. The mean annual temperatures in Yangon/Bangkok and Shillong are 28 ˚C and 18 ˚C, respectively. The temperature effect on speleothem $\delta^{18}O$ during calcite precipitation (-0.21‰/˚C, *(25)*) leads to an approximately 2.1‰ shift, and therefore, can account for the observed offset.

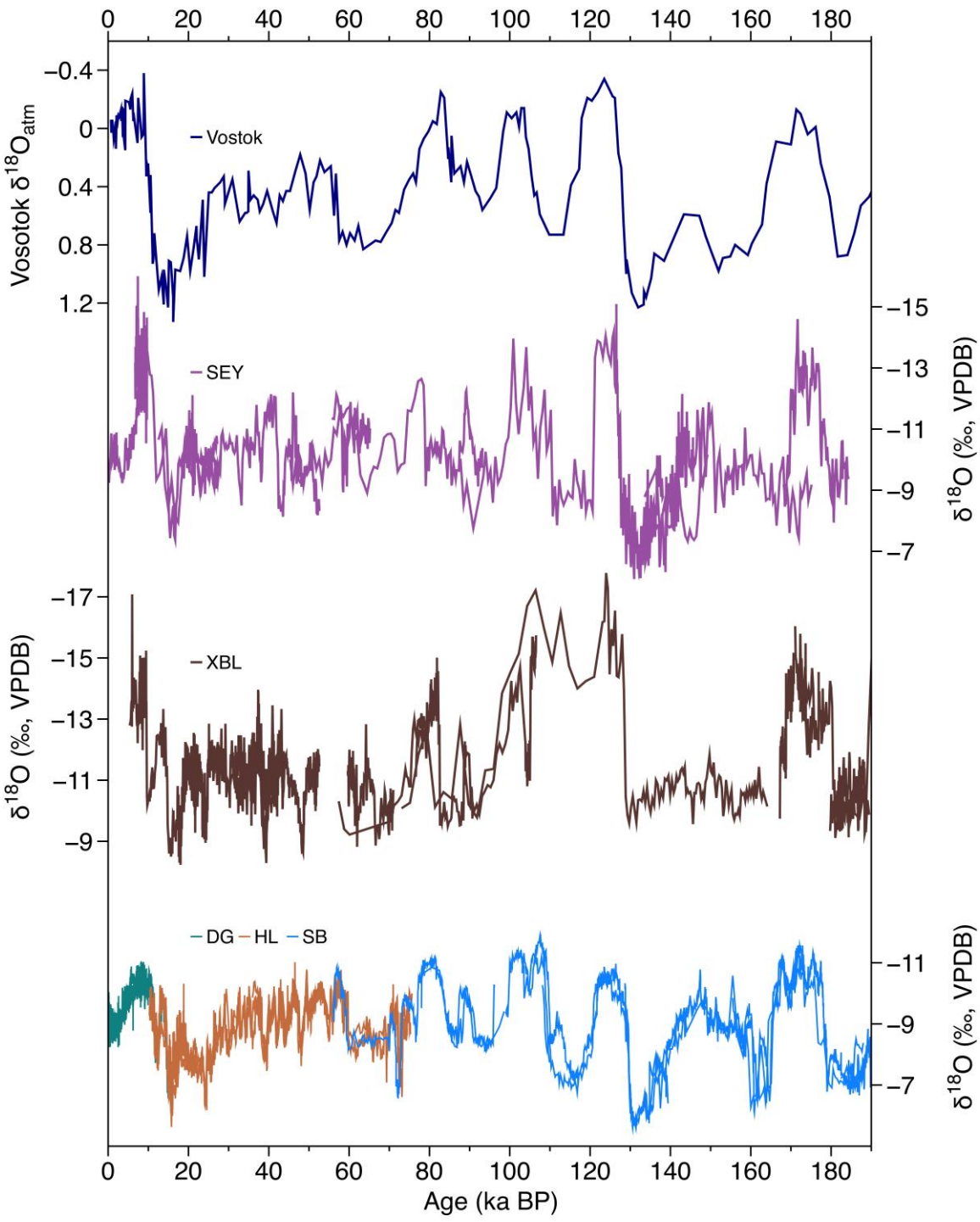

Fig. S9. Comparison of orbital AM records and Vostok atmospheric molecular oxygen $\delta^{18}O$ record. Dark blue: the atmospheric molecular oxygen $\delta^{18}O$ record from Vostok ice core, Antarctica *(86)*; purple: speleothem $\delta^{18}O$ records from SEY caves; dark brown: speleothem $\delta^{18}O$ records Xiaobailong cave *(20)*; green-brown-blue: combined speleothem

$\delta^{18}O$ records from southern China's Hulu cave, HL *(2, 60)*, Dongge cave, DG *(61, 62)*, and Sanbao cave, SB, in which the Sanbao record was shifted positively by 1.6‰ to align it with the other two cave records *(1)*.

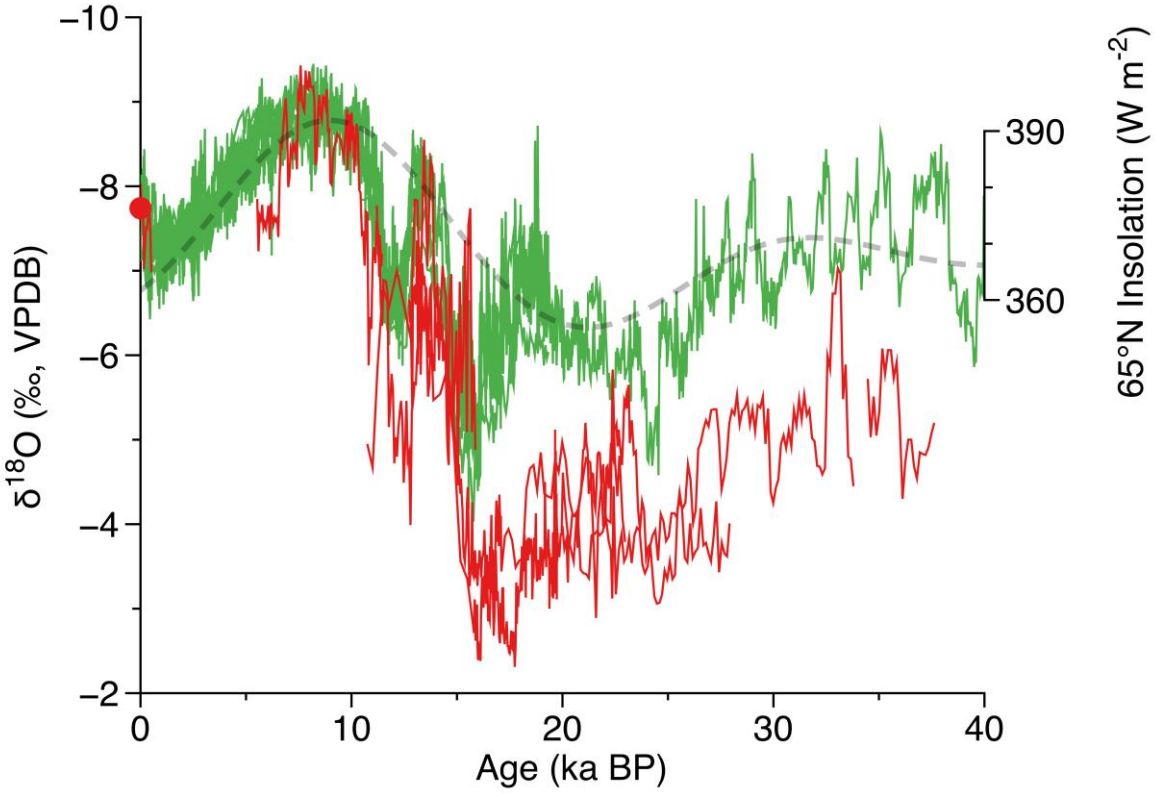

Fig. S10. Spatial-temporal comparison of speleothem $\delta^{18}O$ records from the coastal Indian Ocean and southern China. The red line and red dot represent the compiled record from this study together with the Mawmluh cave record *(21, 26)* corrected for temperature effect (Fig. S8). The green line is a compiled speleothem $\delta^{18}O$ record from Hulu cave *(2, 60)*, Dongge cave *(61, 62)*, and Sanbao cave, with the Sanbao record shifted positively by 1.6‰ to align it with the Hulu and Dongge records *(1)*. The thick grey line shows the 65°N summer insolation. The Chinese records show very small differences in $\delta^{18}O$ between the late Holocene and the LGM. Much larger differences observed in the Indian Ocean coastal records, however, cannot be explained by insolation changes alone.

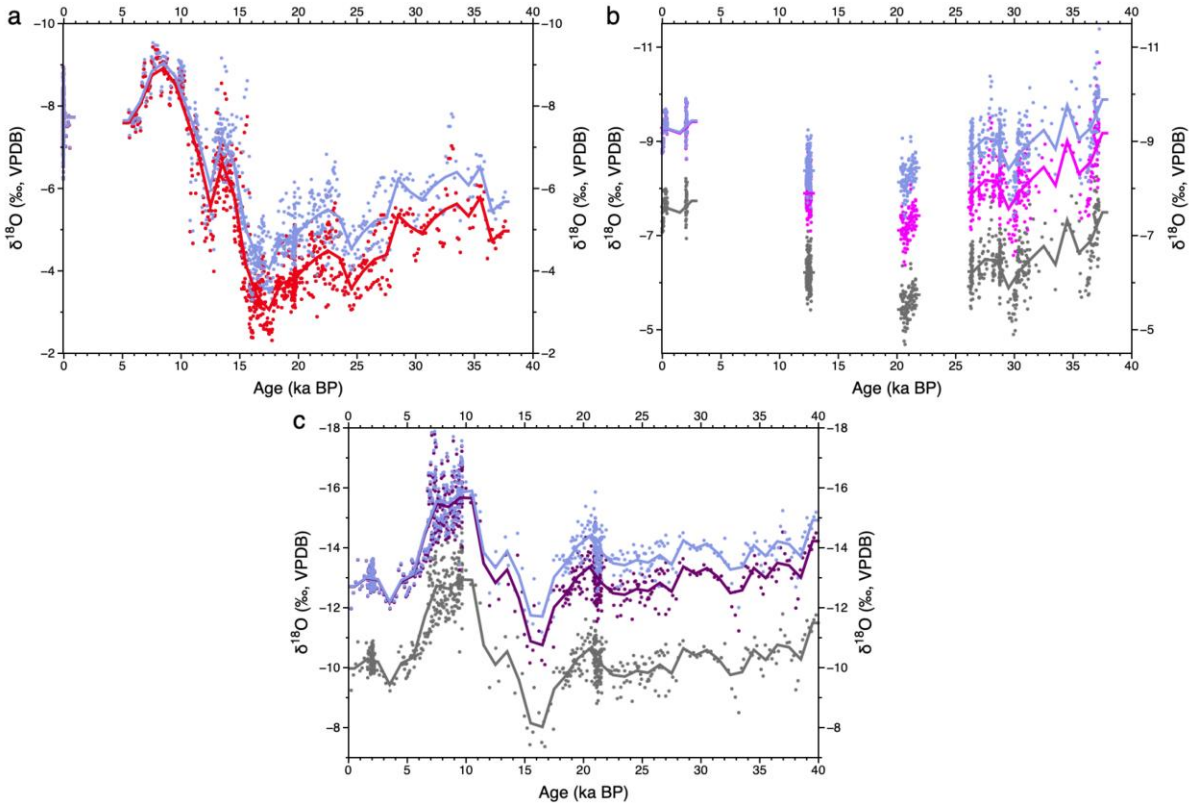

Fig. S11. Ice volume and temperature effects. a). Ice volume effect on the CBoB and Mawmluh $\delta^{18}O$ records. The red dots represent the compiled record from this study together with the Mawmluh cave record *(21, 26)* corrected for temperature effect (Fig. S8). The light blue dots show the records after ice-volume correction, which was done by subtracting global seawater $\delta^{18}O$ (ice volume effect), derived from the updated global sea level model *(87)*. We further calculated the trend line using 1,000-yr averages (thick lines). Note that a large $\delta^{18}O$ shift (~2.7 ‰) still exists between the LGM and modern values. **b).** Effects of cave temperature and ice volume on the CM $\delta^{18}O$ record. The original data are in grey. The pink dots show the record after correcting for cave temperature effect (a ~-1.7‰ shift to account for a ~8 °C temperature difference relative to the CBoB). The light blue dots show the record after ice-volume correction, which was done by subtracting global seawater $\delta^{18}O$ (ice volume effect), derived from the updated global sea level model *(87)*. We further calculated the trend line using 1,000-yr averages (thick lines). Note that a slight $\delta^{18}O$ shift (~1‰) still exists

between the LGM and modern values, even after correcting for cave temperature and ice volume effects. **c).** Effects of cave temperature and ice volume on the SEY $\delta^{18}O$ records. The original data are in grey. The purple dots show the record after correcting for cave temperature effect (a ~-2.7‰ shift to account for a ~13 °C temperature difference relative to the CBoB). The light blue dots show the record after ice-volume correction, which was done by subtracting global seawater $\delta^{18}O$ (ice volume effect), derived from the updated global sea level model *(87)*. We further calculated the trend line using 1,000-yr averages (thick lines). Note that after the two corrections, LGM $\delta^{18}O$ is similar or even lower than the modern values.

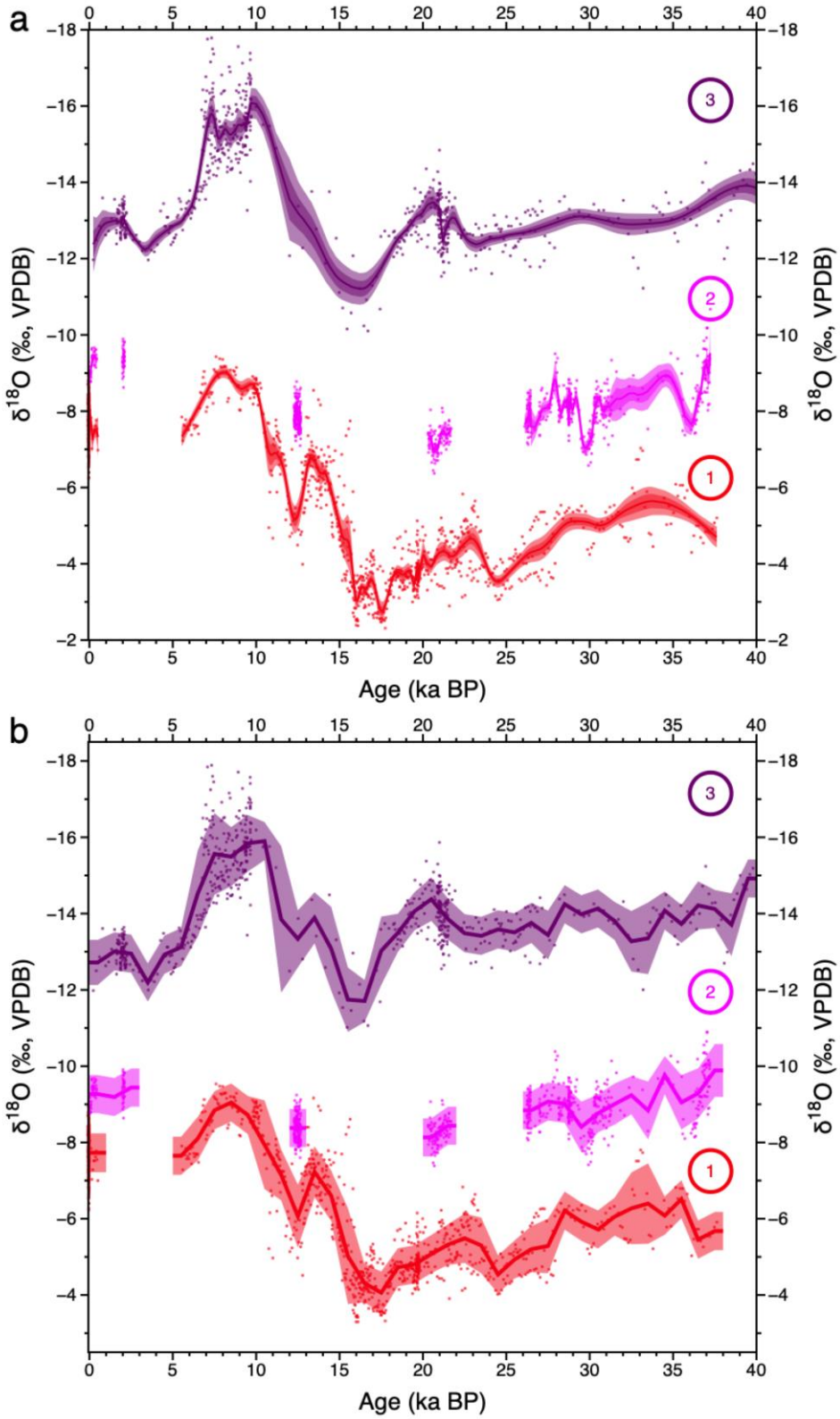

Fig. S12. Spatial-temporal comparison of speleothem $\delta^{18}O$ records from mainland Southeast Asia over the past 40 ka. a). Regression analysis on the three records after temperature correction. We smoothed the records with a 5% LOESS regression method using

the Bootstrap function in ACYCLE 1.2 *(88)*. The number of bootstrap samplings was 1,000. The records obtained from CBoB and Mawmluh *(21, 26)* (site 1), CM LNT (site 2), and SEY caves (site 3) are shown in red, pink, and purple, respectively. The shaded envelopes indicate the range of 1σ and 2σ uncertainty of the $\delta^{18}O$ values. The smoothed records indicate the general spatial-temporal pattern of speleothem $\delta^{18}O$ records from mainland Southeast Asia over the past 40 ka. Note that for the SEY record, the smoothed record was slightly biased to its high resolution portion (e.g., ~7 ka). **b).** Comparison of the three records after ice-volume correction. The ice volume effect contributes equally to rainfall $\delta^{18}O$ at all the cave sites. The corrected records bear identical gradients between cave sites as in the original records, although the $\delta^{18}O$ shift between the LGM and the present day becomes smaller in each individual record (Fig. 4).

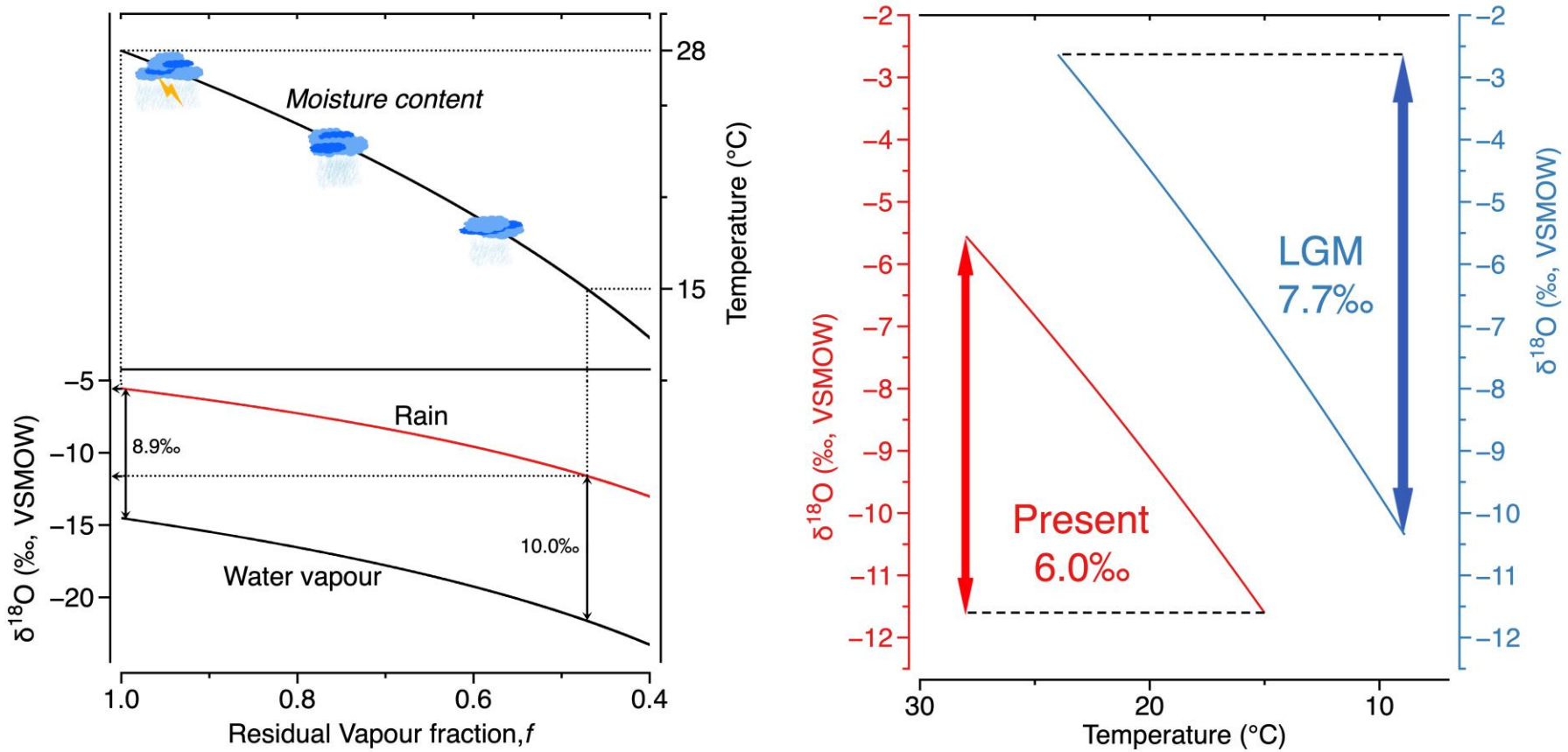

Fig. S13. Calculation of rainfall $\delta^{18}O$ gradient across mainland Southeast Asia. (modified from *(89)*): the changes in $\delta^{18}O$ of rainfall and water vapor according to an idealized temperature-dependent Rayleigh fractionation model, starting with $\delta^{18}O_{vi}$ = -14.5‰ ($\delta^{18}O_{pi}$ = -5.6‰, Table S3), and temperature = 28 °C (representing modern climate conditions at CBoB). **Right,** a comparison of rainfall $\delta^{18}O$ gradient changes between

the present day and the LGM according to idealized temperature-dependent Rayleigh fractionation models. The red curve starts with $\delta^{18}O_{vi}$ = -14.5‰ ($\delta^{18}O_{pi}$ = -5.6‰, Table S3), temperature = 28 °C, and final temperature = 15 °C; and the blue curve starts with $\delta^{18}O_{vi}$ = -12.0‰ ($\delta^{18}O_{pi}$ = -2.6‰, Table S3), temperature = 24 °C, and final temperature = 9 °C. The figure conceptually illustrates the rainfall $\delta^{18}O$ change with temperature drop in mainland Southeast Asia for a present-day scenario and a hypothetical LGM scenario. For the present day, we start with $\delta^{18}O_{pi}$ = -5.6‰ (Table S3), and temperature = 28 °C at the coastal site. When the temperature drops to 15 °C at the SEY site, $\delta^{18}O_p$ evolves to -11.6‰. During the LGM, we assume a 4 °C cooling in the coastal region (i.e., 24 °C). With an initial rainfall $\delta^{18}O_{pi}$ of -2.6‰ (Table S3), rainfall $\delta^{18}O_p$ would have decreased to -9.2‰ at the SEY site if temperature gradient was similar to today, but would have further dropped to -10.3‰ if the temperature gradient increased modestly by ~2 °C/1,000 km (i.e., to 9 °C at SEY). Note that the calculated difference of 6.0‰ in rainfall $\delta^{18}O$, caused by a temperature drop from 28 °C at the CBoB to 15 °C at SEY, is larger than the modern offset between the corrected speleothem $\delta^{18}O$ values from the two sites (5.2±0.7‰ VPDB, Fig. 4) or the modern offset between the speleothem inferred rainfall $\delta^{18}O$ values from the two sites (5.1±0.7‰ VSMOW, Table S2). This small discrepancy is consistent with a dominant transpiration process in moisture recycling today *(90, 91)*, and it might also suggest a somewhat overestimated temperature effect on speleothem $\delta^{18}O$ or an underestimated stronger eddy diffusion effect. On the other hand, the calculated decrease of 7.7‰ in rainfall $\delta^{18}O$ during the LGM is smaller than the offset of ~9‰ in the corrected speleothem $\delta^{18}O$ records during 19-23 ka (Fig. 4), suggesting that temperature alone is not sufficient to account for the difference in the isotope gradient between the glacial time and the present day across mainland Southeast Asia. Therefore, changes in moisture recycling process must have been involved.

Supplementary Tables

Table S1. A list of the studied speleothem samples and their cave locations.

Coastal Bay of Bengal (CBoB)		Central Myanmar (CM)		Southeast Yunnan (SEY)	
Caves	Samples	Caves	Samples	Caves	Samples
Hin Tum No.2 Cave (HT2) 15°01.272' N, 99°26.757' E	HT2-1, HT2-2	Lin Noe Twin Cave (LNT) 21°14.223' N, 96°26.625' E	LNT01, LNT02, LNT04, LNT05, LNT09	Baifen Cave (BF)	BF2
				Jiangjun Cave (JJ)	JJ03, JJ06
Phabaung Gu Cave (PHA) 16°17.210' N, 97°54.092' E	PHA02 (actively growing)			Shuanglong Cave (SL)	SL08, SL10
				Shuiyuan Cave (SY)	SY10
Padamya Gu Cave (PDM) 16°49.725' N, 97°42.369' E	PDM02			Xianren Cave (XR)	XR05
				Unnamed Cave (A) ~23.5°N, ~104°E (The exact GPS coordiantes of SEY caves were not taken.)	A14 (aragonite), A15
Ya Thea Pyan Gu (YTP) 16°50.107' N, 97°34.245' E	YTP01				

Table S2. Rainfall oxygen isotopic compositions across mainland Southeast Asia. Note here that: (1) the modern rainfall $\delta^{18}O$ values (VSMOW) of Bangkok and Kunming are measured by IAEA (Data from: https://nucleus.iaea.org/wiser/index.aspx); (2) the modern rainfall $\delta^{18}O$ value (VSMOW) of Taunggyi is calculated from IsoMap (http://wateriso.utah.edu/waterisotopes/pages/data_access/oipc.html) *(65)*; and (3) the mean modern speleothem $\delta^{18}O$ value at each location (VPDB) is the average value of speleothem $\delta^{18}O$ that are younger than 1 ka, and the minimum 1σ standard deviation is assumed to be 0.5‰, as smaller standard deviations could be resulted from relatively sparse data points.

	Modern rainfall $\delta^{18}O$ (VSMOW)	Mean annual temperature (°C)		Mean modern speleothem $\delta^{18}O$ (VPDB)	Speleothem inferred rainfall $\delta^{18}O$ (VSMOW)
Bangkok	-6.7‰ (n=40, 1σ=1.0)	~28	CBoB	-7.5‰ (n=12, 1σ=0.5)	-5.6‰ (1σ=0.5)
Taunggyi	-7.6‰	~20	CM	-7.6‰ (n=40, 1σ=0.5)	-7.2‰ (1σ=0.5)
Kunming	-10.4‰ (n=13, 1σ=1.0)	~15	SEY	-10.0‰ (n=5, 1σ=0.5)	-10.7‰ (1σ=0.5)

Table S3. Calculations of water vapor loss over the CBoB site. Note here that for the calculated $\delta^{18}O_c$, the minimum 1σ standard deviation is assumed to be 0.5‰, as smaller standard deviations could be resulted from relatively sparse data points.

Time Interval	Cave temperature (°C)	$\delta^{18}O_c$ (‰, VPDB)	$\delta^{18}O_{sw}$ (‰, VSMOW)	$\delta^{18}O_p$ (‰, VSMOW)	Water vapor remaining in air mass (%)	Relative Humidity (%)	PWV (kg/m^2)	Amount lost wrt. modern value (%)
Modern	28	-7.5 (n=12, 1σ=0.5)	0	-5.6	54	100	61.9	100
LGM	24	-3.8 (n=145,1σ=0.5)	1	-2.6	68	100	49.5	56
LGM temperaure sensitivity test 1	22	-3.8	1	-3.0	66	100	44.2	54
LGM temperaure sensitivity test 2	26	-3.8	1	-2.2	70	100	55.4	58
Modern	28	-7.5	0	-5.6	54	75	46.4	100
LGM RH senstivity test 1	24	-3.8	1	-2.6	68	75	37.2	56
LGM RH senstivity test 2	24	-3.8	1	-2.6	68	85	42.1	63
LGM RH senstivity test 3	24	-3.8	1	-2.6	68	90	44.6	67

Data S1. ^{230}Th dating results, with errors within 2σ (95% in confidence). Data S1 is submitted as a separate file.

Data S2. Stable isotope compositions. Data S2 is submitted as a separate file.